Supplement of The Cryosphere, 17, 3063–3082, 2023
https://doi.org/10.5194/tc-17-3063-2023-supplement

The Cryosphere Open Access

Supplement of

Isotopic diffusion in ice enhanced by vein-water flow

Felix S. L. Ng

Correspondence to: Felix S. L. Ng (f.ng@sheffield.ac.uk)

Movies S1–S3: Here, captions only. Access the movies via doi:10.15131/shef.data.21805803

Please use https://figshare.com/s/79e62bdae0f84a2efa11 during the review stage.

Figs. S1–S3

Movie S1. Influence of the vein-water flow velocity w on the pattern of δ in the ice–vein system and on the amount of excess diffusion at T = –32 °C, for a signal with wavelength λ = 0.02 m. These simulations show how the isotopic "shear layer" described in Sect. 3 evolves and transitions between the sheet regime and tail regime as w changes in small steps from –50 m yr^{-1} to 50 m yr^{-1} and back, for the model parameters a = 1 μm, b = 1 mm and α = 1. (a) δ-variations at the vein (red curve) and in the grain interior at $r = b$ (black curve). (b) Colour map of the pattern of δ in the ice. (c) The corresponding decay-rate enhancement factor f (white dot), located on the surface of $f(\lambda, w)$ in Fig. 7a.

Movie S2. Influence of vein-water flow velocity w on the pattern of δ in the ice–vein system and on the amount of excess diffusion at T = –32 °C, for a signal with wavelength λ = 0.08 m. The simulation scheme and layout of panels are the same as in Movie S1.

Movie S3. Compressional scaling of the surfaces of (a) signal decay-rate enhancement factor f, (b) $\log_{10} f$ and (c) signal migration velocity v, over the λ–w parameter space, as temperature decreases from –20 °C to –60 °C. Some axis ranges are updated at –35 °C and –47 °C to focus on relevant variations.

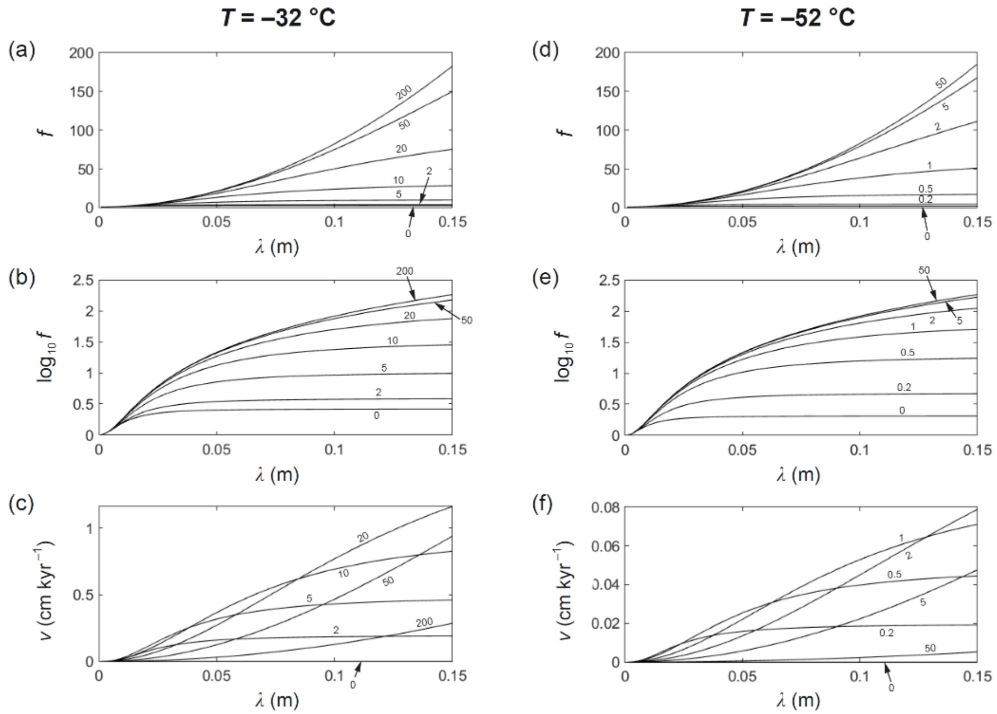

Figure S1. Computed curves of signal decay-rate enhancement factor f, $\log_{10}f$ and signal migration velocity v versus signal wavelength λ, at (a–c) T = –32 °C and (d–f) T = –52 °C, for different vein-water flow velocities w (curve labels in m yr^{-1}) and assuming the deuterium–hydrogen fractionation coefficient, α = 1.021. These curves differ negligibly from those in Fig. 6, where α = 1 is assumed. Results based on the ^{18}O–^{16}O fractionation coefficient, α = 1.0029, are still closer to those in Fig. 6.

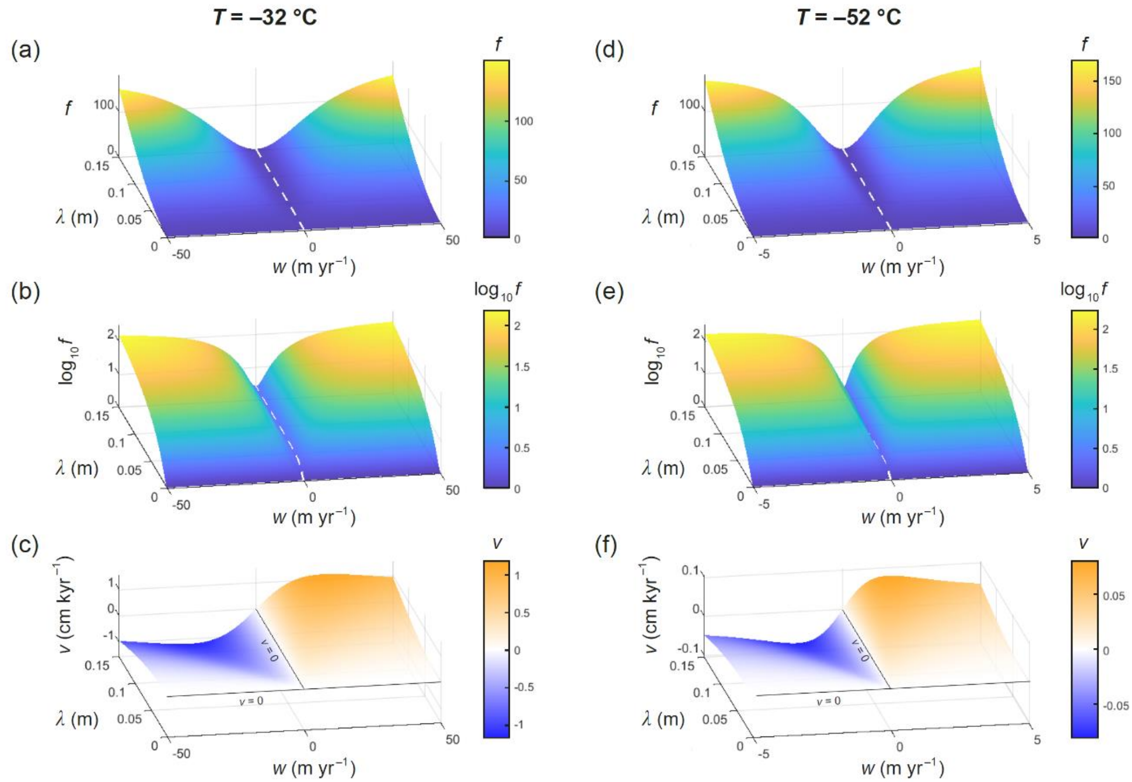

Figure S2. Surfaces of the signal decay-rate enhancement factor f, $\log_{10}f$ and signal migration velocity v over the λ–w parameter space, computed for (a–c) T = –32 °C and (d–f) T = –52 °C and assuming the deuterium–hydrogen fractionation coefficient, α = 1.021. These surfaces differ negligibly from those in Fig. 7, where α = 1 is assumed. Results based on the ^{18}O–^{16}O fractionation coefficient, α = 1.0029, are still closer to those in Fig. 7.

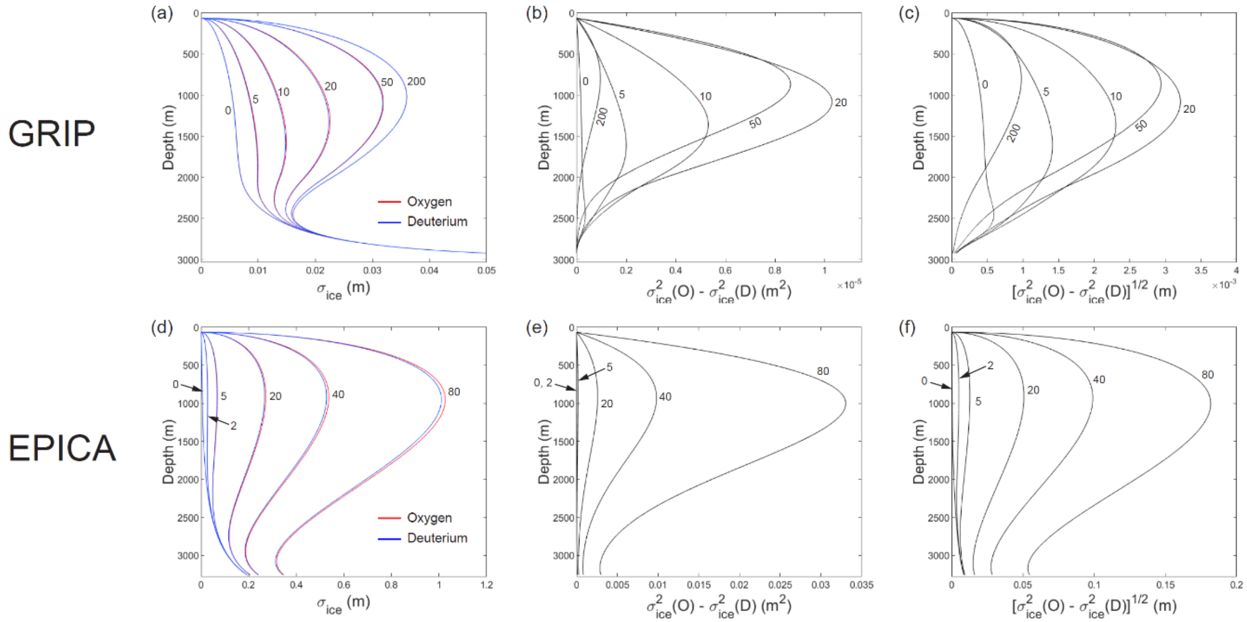

Figure S3. A study of the ice contribution to the differential diffusion length at the (a–c) GRIP and (d–f) EPICA ice-core sites, in model runs using constant grain radius b = 2 mm and different vein-water flow velocities w (curve labels in m yr^{-1}). Depth profiles of (a, d) the ice diffusion lengths σ_{ice}(O) and σ_{ice}(D), (b, e) the square differential $\Delta\sigma_{ice}^2 = \sigma_{ice}^2(O) - \sigma_{ice}^2(D)$, and (c, f) the differential $\Delta\sigma_{ice}$.